Skin Imaging Using Ultrasound Imaging, Optical Coherence Tomography, Confocal Microscopy, and Two-Photon Microscopy in Cutaneous Oncology

Byung Ho Oh[1], Ki Hean Kim[2] and Kee Yang Chung[1]*

[1] Department of Dermatology and Cutaneous Biology Research Institute, Yonsei University College of Medicine, Seoul, South Korea, [2] Department of Mechanical Engineering, Pohang University of Science and Technology, Pohang-si, South Korea

With the recognition of dermoscopy as a new medical technology and its available fee assessment in Korea comes an increased interest in imaging-based dermatological diagnosis. For the dermatologist, who treats benign tumors and malignant skin cancers, imaging-based evaluations can assist with determining the surgical method and future follow-up plans. The identification of the tumor's location and the existence of blood vessels can guide safe treatment and enable the use of minimal incisions. The recent development of high-resolution microscopy based on laser reflection has enabled observation of the skin at the cellular level. Despite the limitation of a shallow imaging depth, non-invasive light-based histopathologic examinations are being investigated as a rapid and pain-free process that would be appreciated by patients and feature reduced time from consultation to treatment. In the United States, the current procedural terminology billing code was established for reflectance confocal microscopy in 2016 and has been used for the skin cancer diagnosis ever since. In this review, we introduce the basic concepts and images of ultrasound imaging, optical coherence tomography, confocal microscopy, and two-photon microscopy and discuss how they can be utilized in the field of dermatological oncology.

Keywords: skin imaging, skin cancer, benign skin tumor, ultrasound, optical coherence tomography, confocal microscopy, two-photon microscopy

INTRODUCTION

Efforts to diagnose skin cancer without skin biopsy are ongoing. The diagnoses of patients with suspected skin cancer are confirmed by punch biopsy followed by histopathological examination, which involve the collection of a small portion of the entire lesion to diagnose skin cancer (1). In this case, since only vertical information of a specific region is acquired, dermoscopy can supplement horizontal information of the entire lesion to identify the most suitable biopsy site. However, dermoscopy has an inherent depth limit confined to the upper dermis (**Table 1**).

TABLE 1 | Pros and cons of skin biopsy and dermoscopy.

	Skin biopsy	Dermoscopy
Advantages	1. Provide universal validity based on long-term accumulated histopathological criteria	1. Identify optimal biopsy sites 2. Reduce unnecessary biopsy 3. Determine horizontal extent of skin lesion 4. Continue to observe lesion treatment
Disadvantages	1. Limitation of evaluating whole lesion by vertical information of specific region 2. Limitations of repeated practice due to pain, bleeding, and infection risk	1. Inherent depth limitation (upper dermis) 2. Difficulty implementing 3D image 3. No reflection of functional and dynamic information (blood flow velocity, oxygen saturation, etc.) of the skin

TABLE 2 | Device resolution and imaging depths[1].

	Resolution	Penetration depth
Confocal microscopy	1 µm	∼500 µm
Optical coherence tomography	2–10 µm	∼2 mm
Ultrasonography	150 µm	∼10 cm
High-resolution computed tomography	300 µm	Entire body
Magnetic resonance imaging	1 mm	Entire body

To observe lesions deep to the upper dermis, the maximum depth that can be observed with dermoscopy, non-invasive techniques, such as confocal microscopy, multiphoton microscopy, optical coherence tomography, and ultrasound must be used. Although each operation principle is different, they all use the reflection characteristic as if it is mirrored, and the skin's depth and resolution differ among device types (**Table 2**). Here we briefly discuss each available device and its clinical use in the dermatology field.

ULTRASOUND IMAGING

Ultrasound imaging uses high-frequency sound waves that cannot be heard by the human ear. When it is sent inside the human body, the degree of absorption and reflection is cut off depending on the constituents and the reflected sound waves are sensed and imaged (2). Therefore, the probe that sends and detects the sound waves forms the core equipment for ultrasound technology. Higher-frequency (MHz) sound waves enable high-resolution observation of the skin surface, but the observable depth decreases. In the field of dermatology, ultrasound is mainly used to identify benign tumor type and extent (**Table 3**). Before surgery, it can provide information about tumor type and size, locate the existence of surrounding vessels, identify the best location for the incision, and set the range while viewing the ultrasound screen in real time with the patient. It can also help the clinician evaluate whether the tumor was completely removed after surgery (**Figure 1**).

In the case of epidermoid cysts, one of the most common benign tumors, it is often seen as a well-defined ovoid-shaped heterogeneous hypoechoic lesion in the subcutaneous layer with strong posterior acoustic enhancement (**Figure 2**). Ultrasonographic findings corresponding to epidermal cyst rupture include pericystic changes, increased vascularity, deep abscess formation, and others (9). Trichilemmal cyst, a benign

appendage lesion derived from the outer root sheath of the hair follicle, is often seen as a well-defined hypoechoic lesion with internal calcification and posterior sound enhancement (**Figure 3**) (8). Identifying these sites just prior to surgery and optimizing the incision site and approach can improve the success rate and reduce recurrence rates.

Pilomatricoma, a benign superficial tumor of the hair follicle, is often seen as a well-defined mass with inner echogenic foci and a peripheral hypoechoic rim or a completely echogenic mass with strong posterior acoustic shadowing in the subcutaneous layer on ultrasonography (**Figure 4**) (7). Pilomatricoma often shows angiographic findings and may be difficult to differentiate from hemangioma.

A lipoma appears as a well-defined hypoechoic mass with multiple echogenic strands on ultrasound (**Figure 5**). If the encapsulation is well-formed, it is easier to remove. Ultrasonography is especially useful for diagnosing and treating lipoma in the forehead. A lipoma occurring in the forehead is often located under the frontalis muscles, and it is important to confirm its precise position using preoperative ultrasonography. It typically has a semispherical shape when located under the muscles and an ovoid shape when it is located in the subcutaneous fat layer (**Figure 6**) (11). However, this is not always the case, so a comprehensive judgment should be made by checking whether it is close to the periosteum or using a special technique that uses the angulation of the probe to point out the lateral borders of the lesion (12).

There are no obvious criteria that can diagnose malignant cutaneous tumors using ultrasound imaging. However, tumor size >5 cm, infiltrated margins, rapid clinical growth, moderate to severe intratumoral hypervascularity (**Figure 7**), and an absence of the typical features of benign tumors are highly suggestive of malignancy (13, 14). High-definition ultrasound with transducers up to 70 MHz, which can observe more detail, has been used to diagnose cutaneous angiosarcoma of the breast and is expected to be useful for the identification of malignant skin cancers (15).

OPTICAL COHERENCE TOMOGRAPHY

Optical coherence tomography (OCT), a three-dimensional (3D) imaging technique based on low coherence interferometry,

Abbreviations: OCT, optical coherence tomography; TPM, two-photon microscopy; EMPD, extramammary Paget's disease; SHG, second harmonic generation; MPM, multi-photon microscopy; BCC, basal cell carcinoma; SCC, squamous cell carcinoma; AK, actinic keratosis.

---

[1]Available online at: http://obel.ee.uwa.edu.au/research/fundamentals/introduction-oct/

TABLE 3 | Key articles comparing ultrasound imaging and histopathology.

Tumor type	Year	Main findings	Correlation with histopathological findings	Probe frequency	Sample size
Basal cell carcinoma (3)	2008	1. BCC tumor ultrasound shows an oval and hypoechoic lesion 2. Compare tumor thickness measurements between ultrasound and histology	Good thickness correlation with histology (intraclass correlation coefficient, 0.9)	7–15 MHz probe	25 patients
Basal cell carcinoma (4)	2007	Lesions that may have a higher aggressive potential may also appear as hyperechoic spots	Hypersonographic spots in BCCs seemed to correspond to calcification, horn cysts, or clusters of apoptotic cells in the centers of nests of basal cell carcinoma	15 or 30 MHz	29 basal cell carcinomas
Invasive squamous cell carcinoma (5)	2009	SCC metastasized to lymph node showed asymmetrical cortical area with high elasticity	Presence of metastatic tumor cells located asymmetrically in a small section of the cortical area	Not mentioned	1 patient
Merkel cell carcinoma (6)	2017	1. Hypoechoic pattern with variable vascularization 2. Useful in the diagnostic work-up of MCC and can help more precisely delimit the tumor prior to complete surgical resection	Not mentioned	18 MHz	7 patients
Pilomatricoma (7)	2005	Well-defined mass with inner echogenic foci and a peripheral hypoechoic rim or a completely echogenic mass with strong posterior acoustic shadowing	Inner echogenic foci may relate with calcification or ossification	7–12 MHz	20 pilomatricomas from 19 patients
Trichilemmal cyst (TC) (8)	2019	Well-defined hypoechoic lesions with internal calcification and posterior sound enhancement	TC contains homogeneous eosinophilic keratinous materials Calcified foci within this keratin can be found	3–12 MHz 6–18 MHz	54 TCs from 50 patients
Ruptured epidermal cyst (REC) (9)	2008	RECs were classified into three types: with lobulations showing echogenic inner contents (type I), with protrusions (type II), and with abscess pocket formations showing poorly defined pericystic changes and increased vascularity around the abscess formation (type III)	Histopathology of the excised RECs also showed similar morphology	5–10 MHz 5–12 MHz	13 patients
Lipoma in the forehead (10)	2016	1. Hyperechoic striated septae parallel to the skin suggestive of lipoma 2. Ultrasonographic findings were accurate in 9 of 14 cases (64.3%).	Unlike the preoperative ultrasonographic findings, 13 of 14 cases were confirmed as frontalis-associated lipomas intraoperatively	12 or 15 MHz	14 patients with lipomas in the forehead

creates an image by detecting the interference phenomena from light scattering or reflection as it passes through different layers of skin via the time domain or Fourier-domain method. OCT non-invasively provides skin images similar to the B mode of ultrasound to a depth of 1–2 mm and a resolution of 2–10 μm with high imaging speed. Functional OCT techniques that can provide additional information, such as polarization and vasculature were recently developed and applied for the detection of abnormal vasculature of a port-wine stain or skin cancer (16–18). Our research group developed a device that matches an OCT image with that obtained by dermoscopic imaging and provides more information than dermoscopy alone (19). Through this, we expect to be able to assess the extent of scar treatment (**Figure 8**). It is expected that a stage of nevus flammeus will be established, and treatment feasibility and degree will be evaluated (**Figure 9**). The limitations of OCT are limited depth of examination and lack of resolution to observe cancer cell morphology. Line-field confocal OCT, which can reveal comprehensive structural mapping of the skin at the cellular level with an isotropic spatial resolution of ∼1 μm to a depth of ∼500 μm, was recently reported to correlate with conventional histopathological images of skin tumors (20). Key articles comparing OCT and histopathology are summarized in **Table 4**.

CONFOCAL MICROSCOPY

Confocal microscopy is based on the existence of one focal point when a laser, used as a light source, is reflected off a subject.
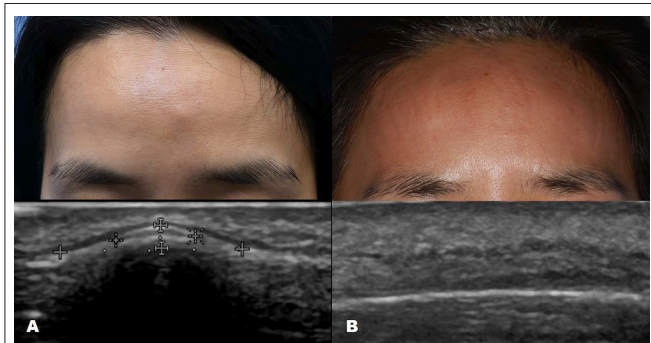

FIGURE 1 | Ultrasound images of forehead osteoma. (A) Before excision. (B) After excision performed through a remote incision above the hairline.

The "out of focus" signal is blocked by a pinhole, and contrast is generated by reflections at the interfaces of tissue and cellular structures due to variations of the index of refraction. Since image acquisition is not possible with a single signal point, imaging occurs by scanning across several pinholes. Imaging up to a depth of 100–200 μm at a 1-μm resolution is possible. Confocal microscopy is capable of providing rapid bedside pathological analysis by producing images with subcellular resolution without skin biopsy and physical sectioning (24–26). There are two ways to use this approach for Mohs surgery. One is used *in vivo* and can help the identification of the surgical margins in a perioperative setting (27). It is also possible to check the remaining lesion using intraoperative images *in vivo* after removing the main skin cancer mass (28). The other is for *ex vivo* use, in which the surgical margins are removed and confocal microscopy is used to confirm whether the tumor remains within it (29). However, when used for detection in Mohs surgery, the grayscale confocal image was difficult to interpret by the surgeons. To improve this, each frozen specimen was stained with acridine orange
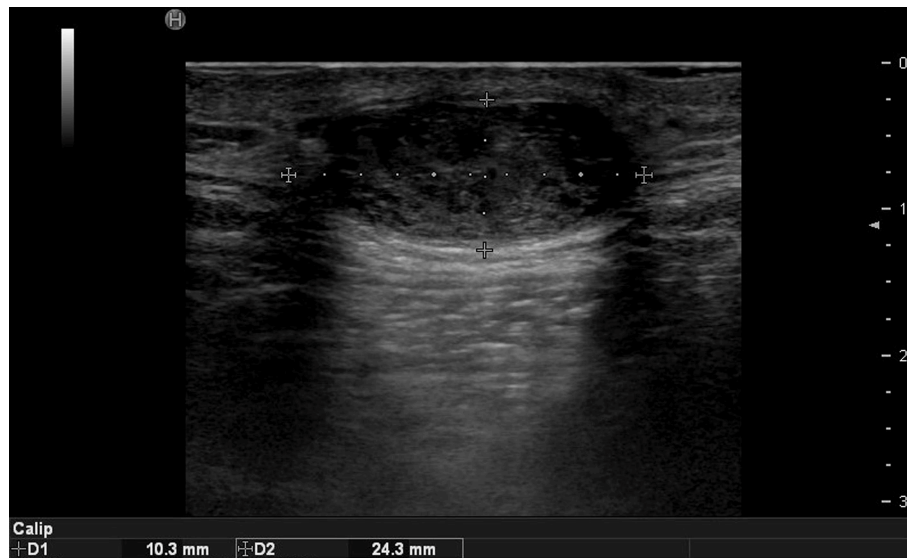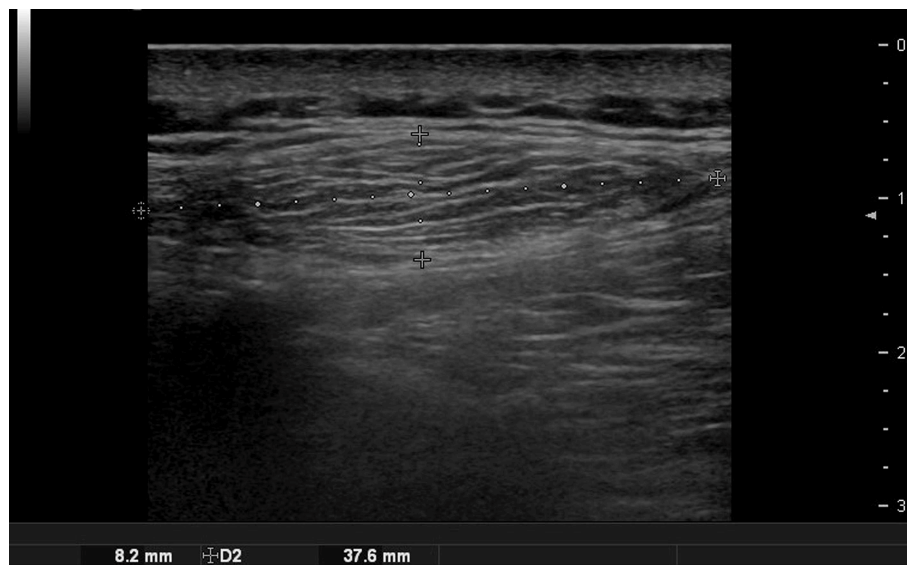

FIGURE 2 | Ultrasound image of epidermal cyst.
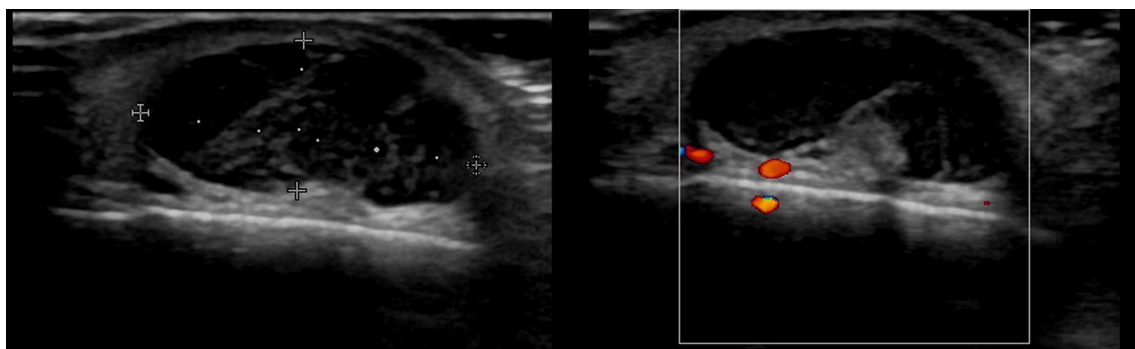
FIGURE 3 | Ultrasound image of trichilemmal cyst.

FIGURE 4 | Ultrasound image of pilomatricoma.

FIGURE 5 | Ultrasound image of lipoma.

(pH 6.0) and eosin (pH 6.0) and then scanned with confocal mosaicking microscopy to imitate hematoxylin and eosin-stained Mohs frozen sections. This approach and physician training can improve the accuracy of the non-melanoma skin cancer diagnosis (30). Key articles comparing confocal microscopy and histopathology are summarized in **Table 5**.

Confocal microscopy has also been applied to diagnose mammary and extramammary Paget's disease (EMPD) (37), frequently showing Paget cells predominantly within the epidermis (38). However, due to the limited depth of imaging (100–200 μm) when applied non-invasively, the invasion site is difficult to determine. A major limitation of this technique is that it can only provide morphological information and does not reflect the tissue's internal structure or functional state.
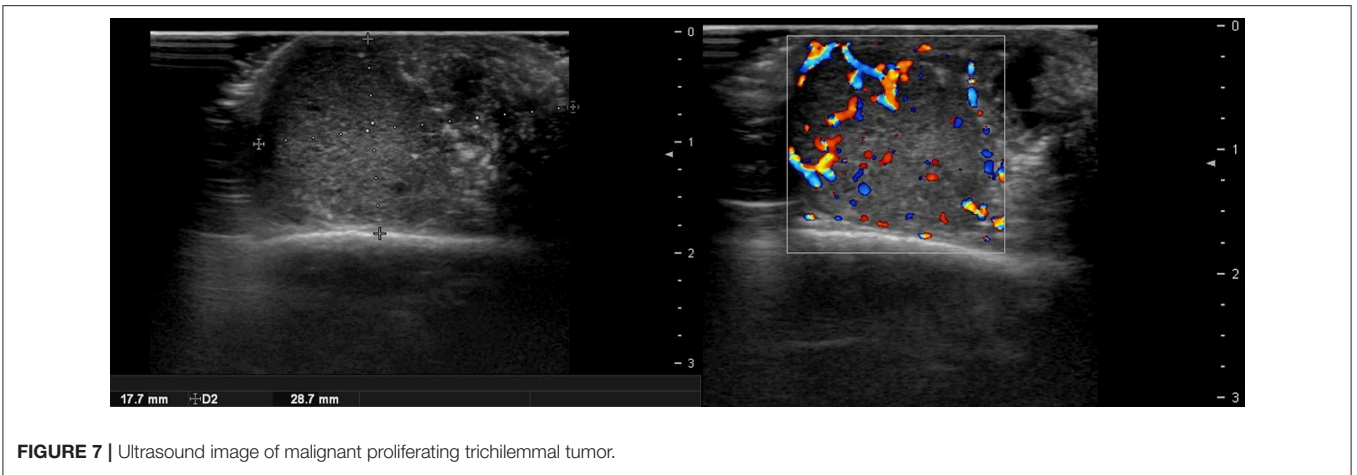
TWO-PHOTON MICROSCOPY

Two-photon microscopy (TPM) is a technique that uses the fluorescence released after excitation from simultaneously
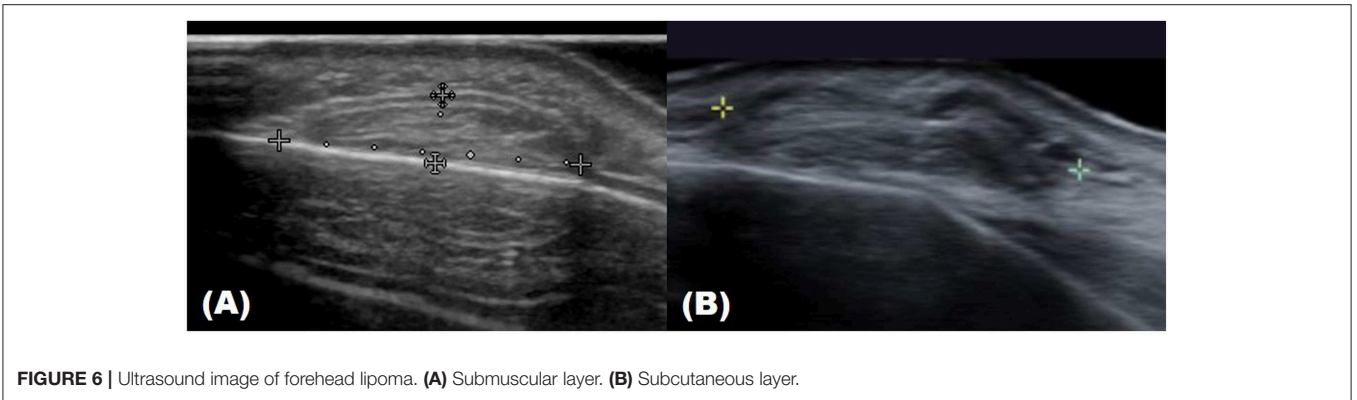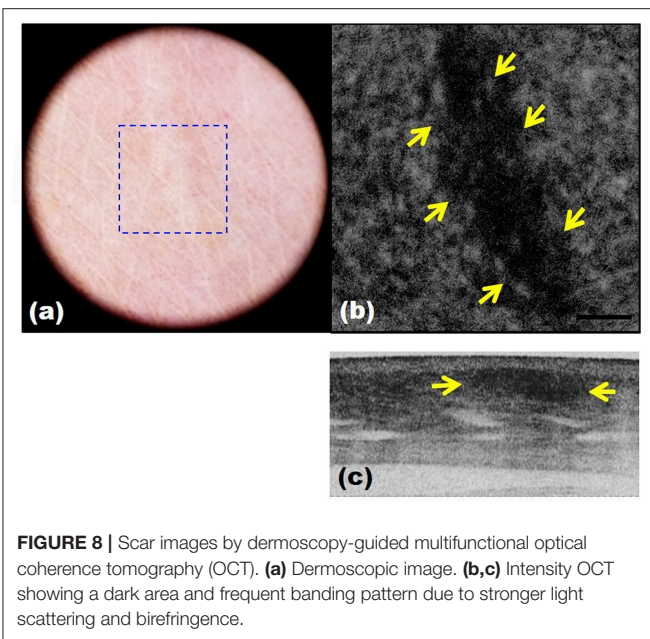
FIGURE 6 | Ultrasound image of forehead lipoma. **(A)** Submuscular layer. **(B)** Subcutaneous layer.

FIGURE 7 | Ultrasound image of malignant proliferating trichilemmal tumor.

FIGURE 8 | Scar images by dermoscopy-guided multifunctional optical coherence tomography (OCT). **(a)** Dermoscopic image. **(b,c)** Intensity OCT showing a dark area and frequent banding pattern due to stronger light scattering and birefringence.
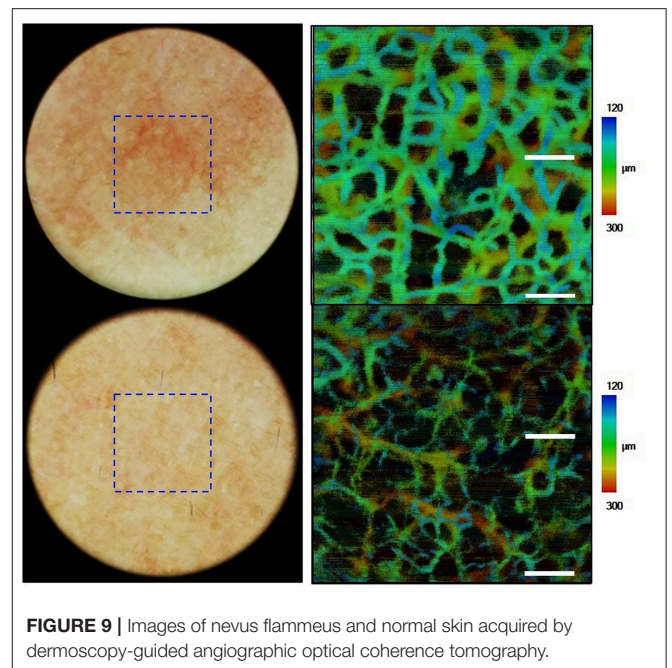
FIGURE 9 | Images of nevus flammeus and normal skin acquired by dermoscopy-guided angiographic optical coherence tomography.

absorbing two photons with long wavelengths and low energy. TPM allows observation of vital phenomena in cells and *in vivo* at the molecular level. In particular, it has the advantage of being able to identify the distribution of collagen within the dermis using the second harmonic generation (SHG) produced when two photons simultaneously interfere. Non-invasive *in vivo*

TABLE 4 | Key articles comparing optical coherence tomography and histopathology.

Tumor type	Year	Type	Main findings	Correlation with histopathology findings	Sample size
Basal cell carcinoma (BCC) (21)	2014	High-definition optical coherence tomography (HD-OCT)	Lobulated nodules, peripheral rimming, epidermal disarray	Peripheral rimming in HD-OCT correlates with peritumoral mucin deposition	25 cases of BCC
BCC (22)	2016	Dynamic OCT enables the detection of blood flow *in vivo* and visualization of the skin microvasculature	Blood vessels varied from dilated, larger-than normal vessels to the smallest detectable vessels	Loose and more vascularized dermis between tumor nests	1 patient with BCC on the cheek
BCC, Melanoma (20)	2018	Line-field confocal OCT	BCC: lobulated structures within the dermis, dark cleft due to mucin deposition; melanoma: general architectural disarrangement, disruption of the dermal-epidermal junction, pagetoid spread of atypical melanocytes	BCC and melanoma approximate shapes observed in OCT appeared similar histopathologically	2 patients with BCC 2 patients with melanoma
Actinic keratosis (AK), Squamous cell carcinoma (SCC) (23)	2015	HD-OCT	Absence of an outlined dermo-epidermal junction on cross-sectional images allowed discriminating SCC from AK and normal skin	It related to irregular budding of the epidermis outstanding into the upper dermis and/or presence of periadenexal collars penetrating through the dermo-epidermal junction	37 cases of AK 16 cases of SCC

TABLE 5 | Key articles comparing confocal microscopy and histopathology.

| Tumor type	Year	Type	Main findings	Correlation with histopathological findings	Sample size
Basal cell carcinoma (BCC) (31)	2002	Real-time, confocal reflectance microscopy (*in vivo*)	Confocal features correlated very well with hematoxylin and eosin (H&E)-stained sections of the biopsy specimen	Features that were readily identified by both *in vivo* confocal microscopy and standard microscopy of H&E-stained sections included parakeratosis, actinic changes overlying the BCC, relative monomorphism of BCC cells, BCC nuclei exhibiting characteristic elongated or oval appearance, high nucleocytoplasmic ratios, and the presence of prominent nucleoli, increased vascularity, and prominent predominantly mononuclear inflammatory cell infiltrate	8 BCC lesions
Actinic keratosis (AK), squamous cell carcinoma (SCC), keratoacanthoma (32)	2009	Reflectance confocal microscopy (*in vivo*)	All 38 cases displayed an atypical honeycomb and/or disarranged pattern of the spinous-granular layer of the epidermis; round nucleated cells were seen in 20 SCCs (65%) and 1 AK (14%) Round blood vessels were seen in the superficial dermis in 28 SCCs (90%) and 5 AKs (72%)	Round nucleated cells at the spinous-granular layer correspond to atypical keratinocytes or dyskeratotic cells	A total of 38 lesions in 24 patients with 7 AKs, 25 SCCs *in situ*, 3 invasive SCCs, and 3 keratoacanthomas
Bowen disease (BD) (33)	2012	Reflectance confocal microscopy (*in vivo*)	Two types of targetoid cells were seen: those presenting as large, homogeneous, bright cells with a dark halo; and round ones with a dark center, surrounding bright rim, and dark halo	Targetoid cells correlated dyskeratotic cells with condensed, eosinophilic cytoplasm and a retraction halo. Dyskeratotic cells were correlated with a dark central nucleus and a surrounding clear retraction halo	10 cases of BD
BCC (34)	2013	Comparison of reflectance confocal microscopy and multiphoton tomography findings (*in vivo*)	Elongated cells and palisading structures are easily recognized using both methods	Due to the higher resolution, changes in nucleus diameter or cytoplasm could be visualized using multiphoton tomography (MPT) Therefore, nucleus diameter, nucleus/cytoplasm ratio, and cell density are estimated for normal and BCC cells using MPT	9 patients with BCC
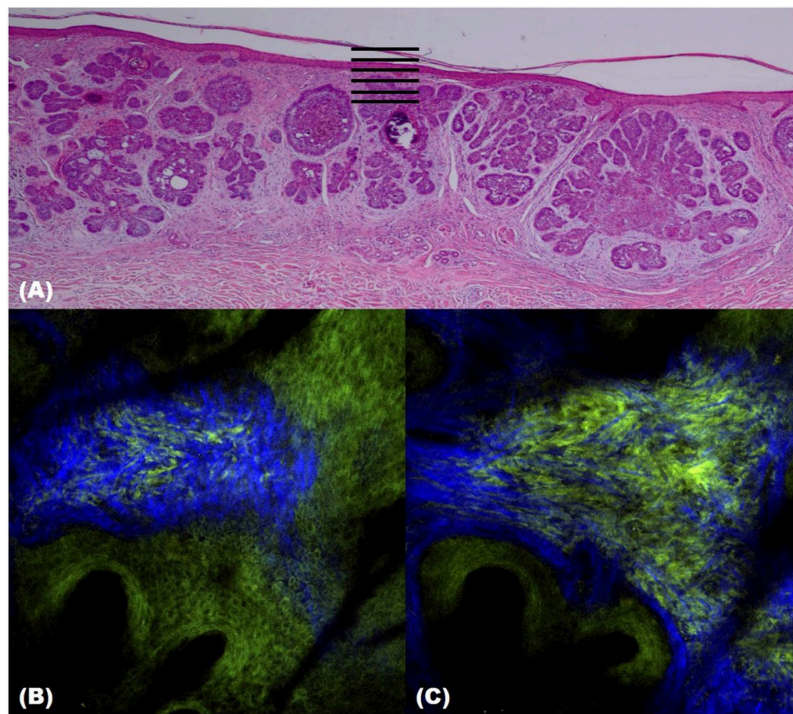
FIGURE 10 | Two-photon microscopy (TPM) images of basal cell carcinoma (BCC). **(A)** Histopathological finding. **(B,C)** TPM images showing parallel collagen fibers (blue) surrounding a BCC tumor nest.

TABLE 6 | Key articles comparing multiphoton microscopy and histopathology.

Tumor type	Year	Type	Main findings	Correlation with histopathological findings	Sample size
Basal cell carcinoma (BCC) (39)	2015	*In vivo* multiphoton microscopy (MPM)	1. Nests of basaloid cells palisading in the peripheral cell layer at the dermoepidermal junction and/or in the dermis 2. Parallel collagen and elastin bundles surrounding the tumors 3. Mucinous stroma adjacent to tumor was visualized using MPM	These features generally correlated well with histopathologic examination. However, histologic examination revealed palisading of peripheral layers in some of the tumor nests of the lesion, although this feature was not obvious in the nests imaged with MPM.	9 patients with a total of 10 BCC
Squamous cell carcinoma *in situ* (SCCIS), superfical BCC (SBCC) (40)	2008	*Ex vivo* MPM	The following findings were seen: SCCIS: bowenoid dysplasia, multinucleated cells, or hyperkeratosis SBCC: peripheral palisading of tumor cells	The morphologic features differed significantly between these lesions and perilesional skin.	5 specimens of SCCIS 6 specimens of SBCC
Actinic keratosis (AK), squamous cell carcinoma (SCC) (41)	2016	*In vivo* MPM	Changes in the morphology of the keratinocytes, such as broadened epidermis, large intercellular spaces, enlarged nucleus and a large variance in cell shape could easily be recognized.	AK: hyperparakeratosis and cell pleomorphism SCC: invasion of the dermis, keratin pearls and hyperchromatic nuclei	6 patients with AK 6 patients with SCC
Benign and malignant melanocytic nevi (BMMN) (42)	2014	*In vivo* MPM	They evaluate BMMN using 9-point scale showing different values according to two-photon excited fluorescence and second harmonic generation of nevi. Indices corresponding to common nevi (0–1), dysplastic nevi (1-4), and melanoma (5-8) were significantly different ($P < 0.05$).	Prominent qualitative correlations included the morphology of epidermal keratinocytes, the appearance of nests of nevus cells surrounded by collagen fibers, and the structure of the epidermal–dermal junction.	5 common nevi 5 dysplastic nevi 5 melanoma
BCC, SCC, dermatofibrosarcoma protuberans (DFSP) (43)	2019	*Ex vivo* moxifloxacin labeling-based MPM	Moxifloxacin MPM imaged both cells and collagen in the skin, similarly to label-free MPM, but with enhanced fluorescence intensities in cells and enhanced imaging speeds.	Moxifloxacin MPM could detect specific cellular features of various skin cancers in good correlation with histopathological images at the higher imaging speed than label-free MPM.	10 patients with BCC 1 patient with SCC 1 patient with DFSP
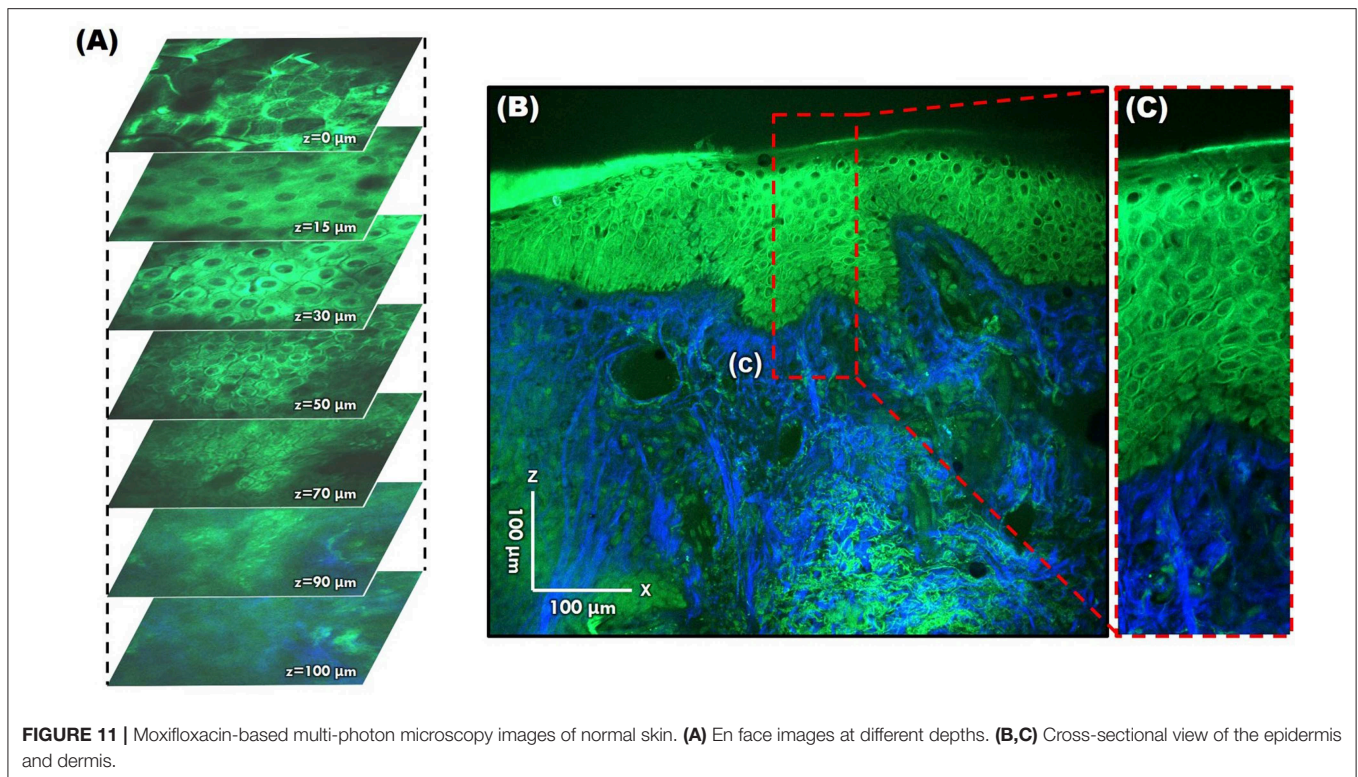
FIGURE 11 | Moxifloxacin-based multi-photon microscopy images of normal skin. **(A)** En face images at different depths. **(B,C)** Cross-sectional view of the epidermis and dermis.

multi-photon microscopy (MPM) imaging also reportedly provides label-free contrast and reveals several characteristic features of basal cell carcinoma lesions (39). This feature correlates well with histopathological examination, findings, and SHG in particular shows collagen and elastin bundles around the tumor (**Figure 10**) (**Table 6**).

However, since TPM and MPM utilize weak endogenous fluorescence in tissue, there is a need for high excitation laser power and extension of pixel duration (44, 45). To overcome this limitation and reduce photodamage, moxifloxacin, an FDA-approved antibiotic, has been reported as a cell-labeling agent for MPM (46). Moxifloxacin has bright intrinsic multi-photon fluorescence, good tissue penetration, and high intracellular concentration. In addition, moxifloxacin-based MPM imaging is 10 times faster than imaging based on endogenous fluorescence (**Figure 11**) (46).

Although imaging depth remains a limitation, various methods to achieve a clear and high-resolution image are being developed. It is also expected that the diagnosis rate can be increased by tumor marker labeling. A recent report stated that in patients with EMPD, a subclinical extension can be assessed by MPM using whole-mount immunostaining with anti-cytokeratin 7 antibody to label Paget cells (35). These trials will be used in the *ex vivo* skin tissue to find the tumor's margins, and it is anticipated that it may replace frozen sections in the future. For more generalized clinical applications, the cost of the equipment is the greatest hinderance. MPM equipment is expensive because it uses a femtosecond laser (36).

CONCLUSION

In addition to ultrasonic devices that can closely observe the skin and deep structures, the development of dermatological equipment that unites laser and optical technology has shown visible progress. The principle of these devices is to analyze signals reflected or scattered from the skin, and there is a fundamental limitation that it is evaluated by looking into the mirror. These limitations are expected to improve in the near future by the development of fluorescent probes targeting tumors or diseases and will be used more actively for the diagnosis and treatment of skin lesions.

For dermatologists, this is a good opportunity to strengthen the specialty of dermatology. We are already familiar with laser equipment and have demonstrated a correlation between clinical and histopathological findings. When we use imaging equipment to further investigate a patient's skin and present objectively explainable data by linking "clinical imaging–histopathological findings," a more robust doctor–patient relationship can be established.

AUTHOR CONTRIBUTIONS

BO conceived the concept and wrote the manuscript. KK co-conceived the concept and drafted the figures and tables. KC co-conceived the concept and edited and improved the manuscript.

REFERENCES

1. Elston DM, Stratman EJ, Miller SJ. Skin biopsy: biopsy issues in specific diseases. *J Am Acad Dermatol.* (2016) 74:1–16; quiz 7–8. doi: 10.1016/j.jaad.2015.06.033

2. Kleinerman R, Whang TB, Bard RL, Marmur ES. Ultrasound in dermatology: principles and applications. *J Am Acad Dermatol.* (2012) 67:478–87. doi: 10.1016/j.jaad.2011.12.016

3. Bobadilla F, Wortsman X, Munoz C, Segovia L, Espinoza M, Jemec GB. Pre-surgical high resolution ultrasound of facial basal cell carcinoma: correlation with histology. *Cancer Imaging.* (2008) 8:163–72. doi: 10.1102/1470-7330.2008.0026

4. Uhara H, Hayashi K, Koga H, Saida T. Multiple hypersonographic spots in basal cell carcinoma. *Dermatol Surg.* (2007) 33:1215–9. doi: 10.1097/00042728-200710000-00009

5. Aoyagi S, Izumi K, Hata H, Kawasaki H, Shimizu H. Usefulness of real-time tissue elastography for detecting lymph-node metastases in squamous cell carcinoma. *Clin Exp Dermatol.* (2009) 34:e744–7. doi: 10.1111/j.1365-2230.2009.03468.x

6. Hernandez-Aragues I, Vazquez-Osorio I, Alfageme F, Ciudad-Blanco C, Casas-Fernandez L, Rodriguez-Blanco MI, et al. Skin ultrasound features of Merkel cell carcinoma. *J Eur Acad Dermatol Venereol.* (2017) 31:e315–8. doi: 10.1111/jdv.14102

7. Hwang JY, Lee SW, Lee SM. The common ultrasonographic features of pilomatricoma. *J Ultrasound Med.* (2005) 24:1397–402. doi: 10.7863/jum.2005.24.10.1397

8. He P, Cui LG, Wang JR, Zhao B, Chen W, Xu Y. Trichilemmal Cyst: clinical and sonographic features. *J Ultrasound Med.* (2019) 38:91–6. doi: 10.1002/jum.14666

9. Jin W, Ryu KN, Kim GY, Kim HC, Lee JH, Park JS. Sonographic findings of ruptured epidermal inclusion cysts in superficial soft tissue: emphasis on shapes, pericystic changes, and pericystic vascularity. *J Ultrasound Med.* (2008) 27:171–6; quiz 7–8. doi: 10.7863/jum.2008.27.2.171

10. Huh JW, Kim MS, Choi KH, Park HJ, Jue MS. The accuracy of ultrasonography on the location of lipomas in the forehead. *Dermatol Surg.* (2016) 42:191–4. doi: 10.1097/DSS.0000000000000598

11. Oh BH, Seo J, Chung KY. Surgical treatment of 846 patients with benign skin tumors: experience of a dermatologic surgeon in Korea. *Korean J Dermatol.* (2015) 53:202–8. Available online at: https://www.koreamed.org/article/0048KJD/2015.53.3.202

12. Wortsman X. The accuracy of ultrasonography on location of lipomas in forehead. *Dermatol Surg.* (2017) 43:158–9. doi: 10.1097/DSS.0000000000000835

13. Chiou HJ, Chou YH, Chiu SY, Wang HK, Chen WM, Chen TH, et al. Differentiation of benign and malignant superficial soft-tissue masses using grayscale and color doppler ultrasonography. *J Chin Med Assoc.* (2009) 72:307–15. doi: 10.1016/S1726-4901(09)70377-6

14. Hung EH, Griffith JF, Ng AW, Lee RK, Lau DT, Leung JC. Ultrasound of musculoskeletal soft-tissue tumors superficial to the investing fascia. *AJR Am J Roentgenol.* (2014) 202:W532–40. doi: 10.2214/AJR.13.11457

15. Perrot JL, Habougit C, Biron Schneider AC, Couzan C, Tognetti L, Rubegni P, et al. Role of reflectance confocal microscopy and HD ultrasound in the diagnosis of cutaneous angiosarcoma of the breast. *Ann Dermatol Venereol.* (2019) 146:410–3. doi: 10.1016/j.annder.2018.12.008

16. Zhao S, Gu Y, Xue P, Guo J, Shen T, Wang T, et al. Imaging port wine stains by fiber optical coherence tomography. *J Biomed Opt.* (2010) 15:036020. doi: 10.1117/1.3445712

17. Mogensen M, Joergensen TM, Nurnberg BM, Morsy HA, Thomsen JB, Thrane L, et al. Assessment of optical coherence tomography imaging in the diagnosis of non-melanoma skin cancer and benign lesions versus normal skin: observer-blinded evaluation by dermatologists and pathologists. *Dermatol Surg.* (2009) 35:965–72. doi: 10.1111/j.1524-4725.2009.01164.x

18. Gambichler T, Plura I, Schmid-Wendtner M, Valavanis K, Kulichova D, Stucker M, et al. High-definition optical coherence tomography of melanocytic skin lesions. *J Biophotonics.* (2015) 8:681–6. doi: 10.1002/jbio.201400085

19. Kwon S, Yoon Y, Kim B, Jang WH, Oh B, Chung KY, et al. Dermoscopy guided dark-field multi-functional optical coherence tomography. *Biomed Opt Express.* (2017) 8:1372–81. doi: 10.1364/BOE.8.001372

20. Dubois A, Levecq O, Azimani H, Siret D, Barut A, Suppa M, et al. Line-field confocal optical coherence tomography for high-resolution noninvasive imaging of skin tumors. *J Biomed Opt.* (2018) 23:1–9. doi: 10.1117/1.JBO.23.10.106007

21. Gambichler T, Plura I, Kampilafkos P, Valavanis K, Sand M, Bechara FG, et al. Histopathological correlates of basal cell carcinoma in the slice and en face imaging modes of high-definition optical coherence tomography. *Br J Dermatol.* (2014) 170:1358–61. doi: 10.1111/bjd.12797

22. Ulrich M, Themstrup L, de Carvalho N, Manfredi M, Grana C, Ciardo S, et al. Dynamic optical coherence tomography in dermatology. *Dermatology.* (2016) 232:298–311. doi: 10.1159/000444706

23. Boone MA, Marneffe A, Suppa M, Miyamoto M, Alarcon I, Hofmann-Wellenhof R, et al. High-definition optical coherence tomography algorithm for the discrimination of actinic keratosis from normal skin and from squamous cell carcinoma. *J Eur Acad Dermatol Venereol.* (2015) 29:1606–15. doi: 10.1111/jdv.12954

24. Rajadhyaksha M, Grossman M, Esterowitz D, Webb RH, Anderson RR. *In vivo* confocal scanning laser microscopy of human skin: melanin provides strong contrast. *J Invest Dermatol.* (1995) 104:946–52. doi: 10.1111/1523-1747.ep12606215

25. Ulrich M, Lange-Asschenfeldt S. *In vivo* confocal microscopy in dermatology: from research to clinical application. *J Biomed Opt.* (2013) 18:061212. doi: 10.1117/1.JBO.18.6.061212

26. New K, Petroll WM, Boyde A, Martin L, Corcuff P, Leveque J, et al. *In vivo* imaging of human teeth and skin using real-time confocal microscopy. *J Scan Microsc.* (1991) 13:369–72. doi: 10.1002/sca.4950130507

27. Couty E, Tognetti L, Labeille B, Douchet C, Habougit C, Couzan C, et al. *In vivo* reflectance confocal microscopy combined with the 'spaghetti technique' for the identification of surgical margins of lentigo maligna: experience in 70 patients. *J Eur Acad Dermatol Venereol.* (2018) 32:e366–8. doi: 10.1111/jdv.14947

28. Flores ES, Cordova M, Kose K, Phillips W, Rossi A, Nehal K, et al. Intraoperative imaging during Mohs surgery with reflectance confocal microscopy: initial clinical experience. *J Biomed Opt.* (2015) 20:61103. doi: 10.1117/1.JBO.20.6.061103

29. Cinotti E, Perrot JL, Labeille B, Cambazard F, Rubegni P. *Ex vivo* confocal microscopy: an emerging technique in dermatology. *Dermatol Pract Concept.* (2018) 8:109–19. doi: 10.5826/dpc.0802a08

30. Mu EW, Lewin JM, Stevenson ML, Meehan SA, Carucci JA, Gareau DS. Use of digitally stained multimodal confocal mosaic images to screen for nonmelanoma skin cancer. *JAMA Dermatol.* (2016) 152:1335–41. doi: 10.1001/jamadermatol.2016.2997

31. Gonzalez S, Tannous Z. Real-time, *in vivo* confocal reflectance microscopy of basal cell carcinoma. *J Am Acad Dermatol.* (2002) 47:869–74. doi: 10.1067/mjd.2002.124690

32. Rishpon A, Kim N, Scope A, Porges L, Oliviero MC, Braun RP, et al. Reflectance confocal microscopy criteria for squamous cell carcinomas and actinic keratoses. *Arch Dermatol.* (2009) 145:766–72. doi: 10.1001/archdermatol.2009.134

33. Ulrich M, Kanitakis J, Gonzalez S, Lange-Asschenfeldt S, Stockfleth E, Roewert-Huber J. Evaluation of Bowen disease by *in vivo* reflectance confocal microscopy. *Br J Dermatol.* (2012) 166:451–3. doi: 10.1111/j.1365-2133.2011.10563.x

34. Ulrich M, Klemp M, Darvin ME, Konig K, Lademann J, Meinke MC. *In vivo* detection of basal cell carcinoma: comparison of a reflectance confocal microscope and a multiphoton tomograph. *J Biomed Opt.* (2013) 18:61229. doi: 10.1117/1.JBO.18.6.061229

35. Murata T, Honda T, Egawa G, Kitoh A, Dainichi T, Otsuka A, et al. Three-dimensional evaluation of subclinical extension of extramammary Paget disease: visualization of the histological border and its comparison to the clinical border. *Br J Dermatol.* (2017) 177:229–37. doi: 10.1111/bjd.15282

36. Tkaczyk E. Innovations and developments in dermatologic non-invasive optical imaging and potential clinical applications. *Acta Derm Venereol.* (2017) 218:5–13. doi: 10.2340/00015555-2717

37. Cinotti E, Galluccio D, Tognetti L, Habougit C, Manganoni AM, Venturini M, et al. Nipple and areola lesions: review of dermoscopy and reflectance confocal microscopy features. *J Eur Acad Dermatol Venereol.* (2019) 33:1837–46. doi: 10.1111/jdv.15727

38. Gonzalez S, Sanchez V, Gonzalez-Rodriguez A, Parrado C, Ullrich M. Confocal microscopy patterns in nonmelanoma skin cancer and clinical applications. *Actas Dermosifiliogr.* (2014) 105:446–58. doi: 10.1016/j.adengl.2014.04.007

39. Balu M, Zachary CB, Harris RM, Krasieva TB, Konig K, Tromberg BJ, et al. *In vivo* multiphoton microscopy of basal cell carcinoma. *JAMA Dermatol.* (2015) 151:1068–74. doi: 10.1001/jamadermatol.2015.0453

40. Paoli J, Smedh M, Wennberg AM, Ericson MB. Multiphoton laser scanning microscopy on non-melanoma skin cancer: morphologic features for future non-invasive diagnostics. *J Invest Dermatol.* (2008) 128:1248–55. doi: 10.1038/sj.jid.5701139

41. Klemp M, Meinke MC, Weinigel M, Rowert-Huber HJ, Konig K, Ulrich M, et al. Comparison of morphologic criteria for actinic keratosis and squamous cell carcinoma using *in vivo* multiphoton tomography. *Exp Dermatol.* (2016) 25:218–22. doi: 10.1111/exd.12912

42. Balu M, Kelly KM, Zachary CB, Harris RM, Krasieva TB, Konig K, et al. Distinguishing between benign and malignant melanocytic nevi by *in vivo* multiphoton microscopy. *Cancer Res.* (2014) 74:2688–97. doi: 10.1158/0008-5472.CAN-13-2582

43. Chang H, Jang WH, Lee S, Kim B, Kim MJ, Kim WO, et al. Moxifloxacin labeling-based multiphoton microscopy of skin cancers in Asians. *Lasers Surg Med.* (2019). doi: 10.1002/lsm.23138. [Epub ahead of print].

44. Thomas G, van Voskuilen J, Gerritsen HC, Sterenborg HJ. Advances and challenges in label-free nonlinear optical imaging using two-photon excitation fluorescence and second harmonic generation for cancer research. *J Photochem Photobiol B.* (2014) 141:128–38. doi: 10.1016/j.jphotobiol.2014.08.025

45. Dela Cruz JM, McMullen JD, Williams RM, Zipfel WR. Feasibility of using multiphoton excited tissue autofluorescence for *in vivo* human histopathology. *Biomed Opt Express.* (2010) 1:1320–30. doi: 10.1364/BOE.1.001320

46. Wang T, Jang WH, Lee S, Yoon CJ, Lee JH, Kim B, et al. Moxifloxacin: clinically compatible contrast agent for multiphoton imaging. *Sci Rep.* (2016) 6:27142. doi: 10.1038/srep27142